Numerical Simulation of 3D–Flow in an Open Channel by Mixing Length Model

Alexey A. Rylov*, Włodzimierz Czernuszenko**

*Institute for Water & Environmental Problems, Barnaul, Russia
**Institute of Geophysics, ul. Ks. Janusza 64, 01–452 Warszawa, Poland

Abstract

A simple turbulence model is applied to close the Reynolds equations for three-dimensional turbulent flow in a rectangular channel. The model is based on the generalisation of Prandtl's mixing length hypothesis which introduces a mixing length tensor. Components of the mixing length tensor are related to the sizes of the largest turbulent eddies. Patankar & Spalding's procedure (1972) is applied to solve the boundary problem for the Reynolds equations numerically. The numerical scheme has overall second order accuracy. It also avoids oscillations in numerical solutions because of holding the maximum principle. The calculated velocity field is compared with data of measurements.

1. Introduction

Numerical modelling of turbulent flows has a long history. In practice it started simultaneously with the appearance of computers. Many turbulence models as well as numerical procedures for fluid mechanics problems were elaborated during this period (Rodi 1980, Fletcher 1991). The turbulence models vary significantly from relatively simple models which do not introduce additional variables and equations to the sophisticated ones including differential equations for each of the individual Reynolds stresses. The latter usually incorporate various empirical constants and functions due to the necessity to parametrize higher-order turbulent moments (e.g. see Lauder, Reece and Rodi 1975, Naot and Rodi 1982).

Engineers dealing with everyday problems would rather have simple but reliable models. In two-dimensional boundary turbulent shear flows the Prandtl's mixing length concept (Schlichting 1955) has been applied with great success for many years. The paper by the authors (Czernuszenko and Rylov 1997) undertakes an attempt to generalize it for three-dimensional flows where mixing length becomes a second rank tensor instead of an original scalar variable within two

dimensions. The problem of turbulence closure therefore shifts to the specification of components of this tensor. Appropriate proposals for these components for flows in rectangular open channels are given in the work mentioned above.

The present article aims to provide a description of the numerical procedure used to implement the model. It is based on the well-known Patankar & Spalding procedure (1972) for parabolic Navier-Stokes equations which are applied to describe three-dimensional flows with specified primary direction.

The formulation of a differential problem is given below, then details of the numerical procedure and results of simulation for rectangular open channel are discussed.

2. Differential Problem Formulation

Bearing in mind the three-dimensional steady flow of fluid in the channel, the problem under consideration consists of the following equations, written with reference to the Cartesian coordinates, x, y, z, which are supposed to be set in streamwise, vertical and spanwise directions, respectively.

Continuity:

$$\frac{\partial u}{\partial x} + \frac{\partial v}{\partial y} + \frac{\partial w}{\partial z} = 0. \tag{1}$$

Momentum:

$$\frac{\partial u^2}{\partial x} + \frac{\partial vu}{\partial y} + \frac{\partial wu}{\partial z} + \frac{1}{\rho}\frac{\partial p}{\partial x} = g\sin\theta + \frac{\partial}{\partial y}\left(\nu_{xy}\frac{\partial u}{\partial y}\right) + \frac{\partial}{\partial z}\left(\nu_{xz}\frac{\partial u}{\partial z}\right), \tag{2}$$

$$\frac{\partial uv}{\partial x} + \frac{\partial v^2}{\partial y} + \frac{\partial wv}{\partial z} + \frac{1}{\rho}\frac{\partial p}{\partial x} = g\cos\theta + \frac{\partial}{\partial y}\left(\nu_{yy}\frac{\partial v}{\partial y}\right) + \frac{\partial}{\partial z}\left(\nu_{yz}\frac{\partial v}{\partial z}\right), \tag{3}$$

$$\frac{\partial uw}{\partial x} + \frac{\partial vw}{\partial y} + \frac{\partial w^2}{\partial z} + \frac{1}{\rho}\frac{\partial p}{\partial z} = \frac{\partial}{\partial y}\left(\nu_{yz}\frac{\partial w}{\partial y}\right) + \frac{\partial}{\partial z}\left(\nu_{zz}\frac{\partial w}{\partial z}\right). \tag{4}$$

In these equations u, v, w stand for mean velocities directed along x, y, z axes, ρ for density, p for pressure, θ for longitudinal channel slope, g for constant of gravity. Various indexed ν denote eddy viscosity coefficients. Terms describing turbulent diffusion in streamwise direction are omitted. These omissions ensure that no influence from downstream can penetrate upstream.

The generalisation of Prandtl's mixing length hypothesis for three-dimensional anisotropic turbulent flows is applied to close the set of equations (1)–(4), (Czernuszenko and Rylov 1997). It is based on triansition from Prandtl's equation in a two-dimensional case

$$-\overline{u'v'} = l^2 \left|\frac{du}{dy}\right|\frac{du}{dy} \tag{5}$$

to its analogue in the space of three dimensions. In the three-dimensional case turbulence may have different length scales in different directions, as it may be

anisotropic, of course. The mixing length in (5) should therefore be replaced by a symmetrical second order tensor (l_{ij}) with dimension of length. The term $|du/dy|$ in three-dimensional space may be replaced by a norm of velocity gradient, and the last multipler on the right hand side of (5) is substituted by the deformation rate tensor $D_{ij} = \partial u_i/\partial x_j + \partial u_j/\partial x_i$. So, equation (5) may be generalized for space of three dimensions in the following way

$$-\overline{u_i' u_j'} = -P_t \delta_{ij} + \frac{1}{2}\left(l_{ik}^2 D_{kj} + l_{jk}^2 D_{ki}\right) S, \tag{6}$$

where $(u_i) = (u, v, w)$, P_t is the "turbulent pressure", S is the norm of velocity gradient, hereafter defined by $S = |\partial u/\partial y| + |\partial u/\partial z|$.

Using (6), eddy viscosity coefficients ν in (2)–(4) may be expressed via the components of a mixing length tensor. Assuming that main axes of the mixing length tensor coincide with coordinate axes, the values of ν may be specified as follows

$$\nu_{ij} = \nu + \frac{1}{2}\left(l_{ii}^2 + l_{jj}^2\right) S, \tag{7}$$

where ν stands for molecular viscosity. Below diagonal non-zero components of (l_{ij}) tensor are denoted by l_x, l_y and l_z. They may be interpreted as Prandtl's mixing lengths in x, y, z directions respectively. For rectangular open channel (Fig. 1) they are modelled by the following multiplicative formulae (Czernuszenko and Rylov 1997)
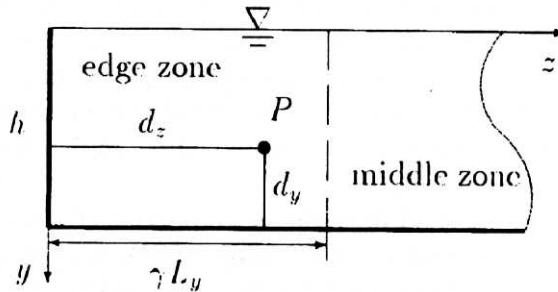

Fig. 1. Experiment S1 conditions, Tominaga et al. (1989)

$$l_y = A_y(d_z) L w(\xi), \tag{8}$$

$$l_z = A_z(d_z) L w(\xi), \tag{9}$$

$$A_y(d) = \begin{cases} L_y Ni\left(\frac{d}{\gamma L_y}\right), & \text{if } \frac{d}{\gamma L_y} < 1 \\ L_y, & \text{else} \end{cases} \tag{10}$$

$$A_z(d) = \begin{cases} L_z Ni\left(\frac{d}{\gamma L_y}\right), & \text{if } \frac{d}{\gamma L_y} < 1 \\ L_z, & \text{else} \end{cases} \tag{11}$$

where functions $Lw(\xi)$, $Ni(\xi)$ refer to the well-known formulae giving mixing length distribution in two-dimensional case

$$\frac{l}{h} = \kappa\sqrt{1-\xi}\left(\frac{1}{\xi} + \pi \Pi \sin(\pi\xi)\right)^{-1} \equiv Lw(\xi), \tag{12}$$

$$\frac{l}{h} = 0.14 - 0.08(1-\xi)^2 - 0.06(1-\xi)^4 \equiv 0.14Ni(\xi), \tag{13}$$

in which $\xi = d_y/h$, κ von Karman constant, Π Coles constant. Equation (12) is derived from the log-wake law for velocity (Nezu and Nakagawa 1993). Formula (13) belongs to Nikuradse (Schlichting 1955).

Quantities A_y, A_z have dimension of length and control the maximal size of turbulent eddies at a vertical. Note that (10)–(11) give the vertical and lateral sizes of the largest eddies proportional to L_y, L_z respectively. Parameter γ controls an interval of increasing eddy sizes from a sidewall in a spanwise direction. In order to get an agreement with two-dimensional mixing length distribution in the channel middle zone far away from the sidewalls we should set

$$l_x = l_y. \tag{14}$$

The equations (1)–(4) are to be accompanied by boundary conditions. They need to be specified along solid boundaries, the water surface and the upstream cross-section bounding the calculation domain. Since the parabolic flows are considered, boundary conditions need not be given at the downstream end of the calculation domain. Furthermore, it is assumed that the cross-sections of the considered channel are rectangles with constant width and depth (rigid lid approximation, Rastogi and Rodi 1978).

The conditions at the solid boundaries were specified using the wall functions technique proposed by Launder and Spalding (1974). According to this technique, the conditions are specified at a point near a wall which lies outside the laminar sublayer and satisfies $30 < y_*y_w/\nu < 100$. It is assumed that the shear stress and the velocity at this grid point satisfy the logarithmic portion of the universal law of the wall

$$\frac{u_w}{u_*} = \frac{1}{\kappa}\ln\frac{u_*y_w}{\nu} + A \tag{15}$$

where u_* friction velocity, y_w distance from the wall, ν molecular viscosity, $A = 5.3$.

Normal velocity components at the solid boundaries and free surface are set at zero. The free surface boundary conditions were specified following the approach of Rastogi and Rodi (1978) which considers the free surface to act as a plane of symmetry. Therefore, the gradients of u and w in y-direction are zeros.

The condition at the initial cross section $x = 0$ for the longitudinal velocity u was taken as logarithmic distribution. Components v and w were set equal to zero.

3. Numerical Procedure

The main idea. The crucial feature of the numerical procedure is uncoupling of longitudinal and lateral pressure gradients, that is the symbol $\bar{p}$ used for the pressure in the x-momentum equations (2) is different from the symbol p in the two other momentum equation. This means that in the procedure an inconsistency is deliberately introduced into the treatment of pressure, and the quantities $\bar{p}$ and p are calculated differently. The pressure $\bar{p}$ can be thought of as a form of space-averaged pressure over a cross-section, and the gradient $(\partial\bar{p}/\partial x)$ is supposed to be known (or calculated) before we proceed to get the lateral pressure gradients $(\partial p/\partial y)$ and $(\partial p/\partial z)$.

If the pressure were known there would be little difficulty: the momentum equations would be uncoupled and could be solved one by one in turn. As it is not known in advance, one can guess the pressures $\bar{p}$ and p, obtain the first approximation to the velocity field, and then make corrections to the pressure in order to bring the velocity field into conformity with the continuity equation.

Approximation to continuity and momentum equations. It utilizes a staggered grid where u_{ijk} and p_{ijk} are defined at points (x_i, y_j, z_k), v_{ijk} – at $(x_i, y_{j-1/2}, z_k)$ and w_{ijk} – at $(x_i, y_j, z_{k-1/2})$. Control Volume (CV) Method is applied to obtain discretized equations. Integrating (1) over the volume depiced in Figure 2, one obtains

$$0 = \int\limits_{C} (u_x + v_y + w_z)dQ =$$

$$= \int\limits_{\Pi bk} udS - \int\limits_{\Pi fr} udS + \int\limits_{\Pi dn} vdS - \int\limits_{\Pi up} vdS + \int\limits_{\Pi rt} wdS - \int\limits_{\Pi lf} wdS = \quad (16)$$

$$= (u^i - u^{i-1})\Delta_{jk} + (v_{j+1} - v_j)\Delta_{i-1/2,k} + (w_{k+1} - w_k)\Delta_{i-1/2j}.$$

Hereafter indices x, y, z at velocity components designate appropriate derivatives,

$$\Delta_i \equiv x_i - x_{i-1}, \Delta_j \equiv y_j - y_{j-1}, \Delta_k \equiv z_k - z_{k-1},$$

$$\Delta_{jk} = \Delta_{j+1/2}\Delta_{k+1/2}, \Delta_{ij} = \Delta_{i+1/2}\Delta_{j+1/2}, \Delta_{ik} = \Delta_{i+1/2}\Delta_{k+1/2},$$

$$\Delta_{ijk} = \Delta_{i+1/2}\Delta_{j+1/2}\Delta_{k+1/2},$$

$\hat{u} \equiv u^i, u = u^{i-1}$ etc., not shifted indices j, k may be omitted. Thus, for example, in Figure 2 $\Delta_{jk}, \Delta_{i-1/2,j}, \Delta_{i-1/2,k}$ give areas of faces $\Pi_{bk}, \Pi_{rt}, \Pi_{dn}$ respectively, and $\Delta_{i-1/2,j,k}$ – a volume of the cube.
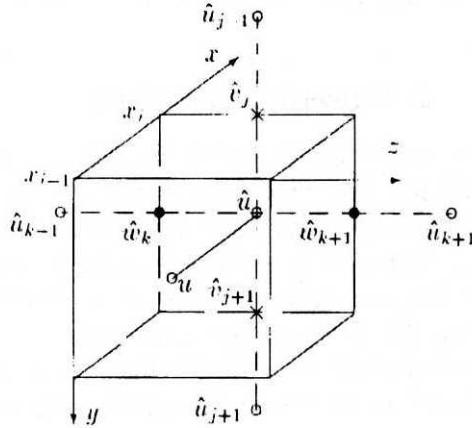
Fig. 2. u–box

Integration of (2) over this cube gives

$$\underset{\Pi_{bk}}{\int} u^2 dS - \underset{\Pi_{fr}}{\int} u^2 dS + \underset{\Pi_{rt}}{\int} vu\, dS - \underset{\Pi l f}{\int} vu\, dS + \underset{\Pi_{dn}}{\int} wu\, dS - \underset{\Pi_{up}}{\int} wu\, dS +$$

$$+\frac{1}{\rho}(\bar{p}_x)_{i-1/2}\Delta_{i-1/2,j,k} = g\sin\theta\,\Delta_{i-1/2,j,k} +$$

$$+ \underset{\Pi_{rt}}{\int} v_y u_y dS - \underset{\Pi_{lf}}{\int} v_y u_y dS + \underset{\Pi_{dn}}{\int} v_z u_z dS - \underset{\Pi_{up}}{\int} v_z u_z dS, \qquad (17)$$

$\bar{p}$ is treated as a scalar in every cross section.

Convective terms are approximated as follows

$$\underset{\Pi_{bk}}{\int} u^2 dS - \underset{\Pi_{fr}}{\int} u^2 dS \approx (\hat{u}u - u^2)\Delta_{jk}, \qquad (18)$$

$$\underset{\Pi_{rt}}{\int} vu\, dS - \underset{\Pi_{lf}}{\int} vu\, dS \approx v_{aver}\frac{\hat{u}_{j+1} - \hat{u}_{j-1}}{2}\Delta_{i-1/2,k} \qquad (19.1)$$

where $v_{aver} = (v_{j+1} + v_j)/2$, for the scheme of the second order accuracy, or

$$\approx \begin{cases} v_{aver}(\hat{u}_j - \hat{u}_{j-1})\Delta_{i-1/2,k}, & \text{if } v_{aver} > 0, \\ v_{aver}(\hat{u}_{j+1} - \hat{u}_j)\Delta_{i-1/2,k}, & \text{if } v_{aver} < 0, \end{cases} \qquad (19.2)$$

for the first order scheme,

$$\underset{\Pi_{dn}}{\int} wu\, dS - \underset{\Pi_{up}}{\int} wu\, dS \approx w_{aver}\frac{\hat{u}_{k+1} - \hat{u}_{k-1}}{2}\Delta_{i-1/2,j} \qquad (20.1)$$

where $w_{aver} = (w_{k+1} + w_k)/2$, for the scheme of the second order accuracy, or

$$\approx \begin{cases} w_{aver} (\hat{u}_k - \hat{u}_{k-1})\Delta_{i-1/2,j}, & \text{if } w_{aver} > 0, \\ w_{aver} (\hat{u}_{k+1} - \hat{u}_k)\Delta_{i-1/2,j}, & \text{if } w_{aver} < 0, \end{cases} \qquad (20.2)$$

for the first order scheme.

Viscous terms are approximated straightforwardly

$$\int\limits_{\Pi_{dn}} v_y u_y dS = \int\limits_{\Pi_{up}} v_y u_y dS \approx$$
$$\approx \left[(v_y)_{j+1/2} \frac{\hat{u}_{j+1} - \hat{u}_j}{\Delta_{j+1}} - (v_y)_{j-1/2} \frac{\hat{u}_j - \hat{u}_{j-1}}{\Delta_j} \right] \Delta_{i-1/2k}, \qquad (21)$$

$$\int\limits_{\Pi_{rt}} v_z u_z dS - \int\limits_{\Pi_{if}} v_z u_z dS \approx$$
$$\approx \left[(v_z)_{k+1/2} \frac{\hat{u}_{k+1} - \hat{u}_k}{\Delta_{k+1}} - (v_z)_{k-1/2} \frac{\hat{u}_k - \hat{u}_{k-1}}{\Delta_k} \right] \Delta_{i-1/2j}. \qquad (22)$$

As two types of the approximation for convective terms have been specified, there should be a rule to choose one of them under each of the specific conditions. The choice depends on the value of the Péclet number representing the ratio of convection to diffusion contribution into the momentum equation. Péclet numbers for this case may be defined as follows

$$Pe_y \equiv v_{aver} \left/ \min \left(\frac{(v_y)_{j+1/2}}{\Delta_{j+1}}, \frac{(v_y)_{j-1/2}}{\Delta_j} \right) \right., \qquad (23.1)$$

and

$$Pe_z \equiv w_{aver} \left/ \min \left(\frac{(v_z)_{k+1/2}}{\Delta_{k+1}}, \frac{(v_z)_{k-1/2}}{\Delta_k} \right) \right.. \qquad (23.2)$$

Second order scheme in $y(z)$-direction is applied if

$$Pe_y \leq 2 \; (Pe_z \leq 2). \qquad (24)$$

Substitution of (18)–(22) into (17) results in the equation

$$(A_0)_{jk}\hat{u}_{jk} - (A_1)_{jk}\hat{u}_{j-1} - (A_2)_{jk}\hat{u}_{j+1} - (A_3)_{jk}\hat{u}_{k-1} - (A_4)_{jk}\hat{u}_{k+1} = F^u_{jk}, \qquad (25)$$

$$\left(F^u_{jk} \equiv -(D^u)_{jk}\bar{p}_x + G^u_{jk} \right),$$

where the term G^u_{jk} incorporates $g \sin \theta$ in equation (2). Nodes arrangement is illustrated by Figure 3. All the coefficients A_s are positive and the equation holds the maximum principle:

$$\sum_{s=1}^{4}(A_s)_{jk} \leq (A_0)_{jk} \qquad (26)$$
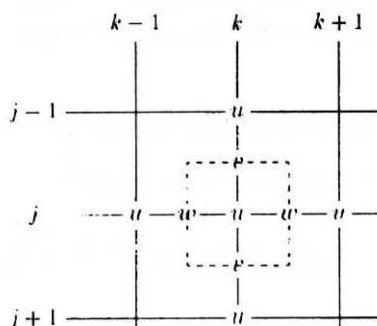
for each j, k.

Fig. 3. Nodes pattern in (24)

The last property guarantees the errors to be bound and the solution of (25) is kept free from any non-physical oscillations. Note that it is holding of the condition (24) which ensures validity of (26).

Treating two other momentum equations (3), (4) in a similar way one gets from (3), (4)

$$(B_0)_{jk}\hat{v}_{jk} - (B_1)_{jk}\hat{v}_{j-1} - (B_2)_{jk}\hat{v}_{j+1} - (B_3)_{jk}\hat{v}_{k-1} - (B_4)_{jk}\hat{v}_{k+1} = F^v_{jk}, \qquad (27)$$

$$(C_0)_{jk}\hat{w}_{jk} - (C_1)_{jk}\hat{w}_{j-1} - (C_2)_{jk}\hat{w}_{j+1} - (C_3)_{jk}\hat{w}_{k-1} - (C_4)_{jk}\hat{w}_{k+1} = F^w_{jk}, \qquad (28)$$

$$\left(F^v_{jk} \equiv -(D^v)_{jk}(\widetilde{p}_{j,k} - \widetilde{p}_{j-1,k}) + G^v_{jk}, \quad F^w_{jk} \equiv -(D^w)_{jk}(\widetilde{p}_{j,k} - \widetilde{p}_{j,k-1}) \right),$$

where $\widetilde{p}_{jk}$ refers to the guessed pressure distribution in the cross section.

Note however that compared to (2) their integration boxes are half-step shifted in the $y(z)$–direction respectively in order to have relevant variable value in the centre of a face normal to the x–direction.

Approximation to Boundary Conditions. Since approximation of Dirichlet-type conditions is trivial, only Neumann-type one is discussed below. Specifically, let us take condition

$$\frac{\partial u}{\partial y} = 0 \quad \text{at surface.} \qquad (29)$$

Approximation to boundary conditions should be chosen of the same order as that to differential equations. Approximation to equations (1)–(4) outlined above has actually the second order of accuracy for the flows with relatively small secondary motion, i.e. components v, w are small compared with u. In order to

have the total second order approximation to the differential problem, let us derive the second order approximation to the surface condition (29) which uses the same 5-point grid pattern as regular difference equations. Applying the CV method, choose a box which is the lower half a regular u–box as shown in Figure 4, and integrate (2) over it
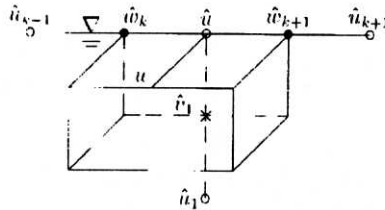

Fig. 4. u-box at surface

$$(u\hat{u} - u^2)\widetilde{\Delta}_{0,k} + \frac{w_k + w_{k+1}}{2}\frac{u_{k+1} + u_{k-1}}{2}\widetilde{\Delta}_{i-1/2,0} +$$

$$+\frac{1}{\rho}(\overline{p}_x)_{i-1/2}\widetilde{\Delta}_{i-1/2,0,k} = g\sin\theta\,\widetilde{\Delta}_{i-1/2,0,k} +$$

$$+\left[(\nu_y)_{1/2,k}\frac{\hat{u}_1 - \hat{u}}{\Delta_1} - (\nu_y)_{0,k}(\hat{u}_y)_{0,k}\right]\widetilde{\Delta}_{i-1/2k} +$$

$$+\left[(\nu_z)_{k+1/2}\frac{\hat{u}_{k+1} - \hat{u}}{\Delta_{k+1}} - (\nu_z)_{k-1/2}\frac{\hat{u} - \hat{u}_{k-1}}{\Delta_k}\right]\widetilde{\Delta}_{i-1/2,0}.$$

Tilded Δ values refer to reduced faces and volume compared to a regular u-box. After replacing $(\hat{u}_y)_{0,k}$ via the boundary condition the second order approximation of it for functions satisfying (2), is obtained.

Numerical Algorithm. Since it is a marching procedure along x-direction, one starts with the given velocity distribution and guessed pressure in the initial cross section, and steps forth till the final x-value.

Each x-step consists of the following substeps. At first, the equation (17) for x-momentum is solved, based on the guessed $(\partial\overline{p}/\partial x)$, as well as (27), (28) for the other momentum, based on the guessed $\widetilde{p}$.

The u-component values $\widetilde{u}^i$, calculated at the next cross section from (25), generally fail to match the initial discharge which can be defined as

$$Q(u) \equiv \sum_{j,k} u_{j,k}\Delta_{j+1}\Delta_{k+1}. \tag{30}$$

So the corrected streamwise velocity

$$u^i = \widetilde{u}^i + \delta u^i \tag{31}$$

which provides the true discharge should be found. Take variation of equation (25), treating terms with $A_s (s = 1, \ldots, 4)$ as small compared to A_0 and omitting them,

$$(A_0)_{jk}(\delta u^i)_{jk} + (D^u)_{jk}\delta \bar{p}_x = 0. \tag{32}$$

Combining (30)–(32) leads to

$$Q_{true} \equiv Q(u^i) = Q(\widetilde{u}^i) + \delta \bar{p}_x \sum_{j,k} \left(-\frac{D^u}{A_0} \right)_{jk} \Delta_{j+1} \Delta_{k+1}. \tag{33}$$

The last relation allows to find correction to longitudinal pressure gradient $\delta \bar{p}_x$. Then, making use of (31) and (32), the improved velocity u^i may be obtained.

Values of $u^i, \widetilde{v}^i, \widetilde{w}^i$ do not satisfy discrete continuity equation (16) so far. The tilded velocity components need to be corrected

$$v^i = \widetilde{v}^i + \delta v^i, \quad w^i = \widetilde{w}^i + \delta w^i. \tag{34}$$

In order to do it variate the discretized v- and w-equation (27), (28). Assuming

$$p = \widetilde{p} + \delta p, \tag{35}$$

similar to (32) one obtains

$$(B_0)_{jk}\delta v_{jk}^i + (D^v)_{jk}(\delta p_j - \delta p_{j-1}) = 0, \tag{36}$$

$$(C_0)_{jk}\delta w_{jk}^i + (D^w)_{jk}(\delta p_k - \delta p_{k-1}) = 0. \tag{37}$$

Substitution of $\delta v_{jk}^i, \delta w_{jk}^i$ from (36), (37) into discretized continuity equation (16) gives an equation for corrections to cross-sectional pressure δ_p

$$(S_0)_{jk}\delta p_{jk} - (S_1)_{jk}\delta p_{j-1} - (S_2)_{jk}\delta p_{j+1} - (S_3)_{jk}\delta p_{k-1} - (S_4)_{jk}\delta p_{k+1} =$$
$$= -Err_{jk}^i(u^i, \widetilde{v}^i, \widetilde{w}^i),$$

where $Err^i(u^i, \widetilde{v}^i, \widetilde{w}^i)$ means residual after substitution $u^i, \widetilde{v}^i, \widetilde{w}^i$ into (16). The last equation also holds maximum principle.

When δp values are found, the formulae (34)–(37) allow to make corrections to the secondary velocities v, w in order to ensure validity of (16) at each inner computational point, and improve p for the next step.

In addition note that despite the fact that the described model has a HYBRYD approximation pattern of convective terms it is actually of the second order of accuracy and thus as accurate as the QUICK scheme f.e. (Leschziner 1980) since secondary velocities appear to be small and it turns on the second order approximation for convective terms.

4. Results and Analysis

The numerical model described was applied to simulate three-dimensional turbulent flow in a rectangular open channel. This choice was supported by the possibility of using experimental velocity distribution measured by Tominaga et al. (1989) in the cross section of the channel. The measurements were carried out in a tilted rectangular open channel at a fully developed flow. Specifications of the case are given in the table below.

Table 1. Experiment S1 conditions, Tominaga et al. (1989)

h	B	u_{mean}	u_{max}	θ
cm	cm	cm s^{-1}	cm s^{-1}	rad
5	40	40.0	46.3	0.94×10^{-3}

To solve the problem for these data, the components of the mixing length tensor should be specified. Knowledge of the macro structure of turbulent eddies helps to do that. In the channel middle zone (far away from the vertical side walls) the largest vertical size of macro eddies should be equal to the water depth, i.e. $L_y = h$. The spanwise size L_z of the largest eddies depends of the bed friction effect which increases with increasing k_s/h and B/h. If bed friction is sufficiently strong, the lateral size of the largest eddies is much smaller than the channel width (Yalin 1992). Parameter L_z is assumed to be equal to the water depth resulting in $L_y = L_z$. Another assumption is related to the size of the edge zone. Because this size is not known a priori, various values of γ have been considered.

Perhaps the most important feature of the measured velocity contours for relatively narrow channels is that the maximal velocity appears not at the surface but rather below it. This occurs due to secondary currents which are directed towards the centre of a channel in the subsurface layer and therefore bring fluid with relatively low momentum from a sidewall to the channel centre. This effect cannot be reproduced by the model since it does not provide explicit proper modelling of the normal Reynolds-stress components. But it is known that anisotropy in $\overline{v'^2}$ and $\overline{w'^2}$ given rise to secondary motion in channel flows. Typical computed isovels are shown in Figure 5.

Figure 6 depicts distribution in a lateral direction computed against measured maximum velocity. Note however, that computed velocity has its maximum at each vertical just at the free surface whereas in experiments the maximum is below it in the marginal zones. Coefficient γ controls the growth rate of the mixing length components from zero at the vertical wall to their maximal values far away from it. The growth is slower for the higher values of γ, i.e. at some distance from the wall for greater γ we have a smaller mixing length, smaller eddy viscosity and greater velocity. Comparison between measured and computed velocity distribution give rise to the conclusion that the best results are achieved for $\gamma = 0.5$.
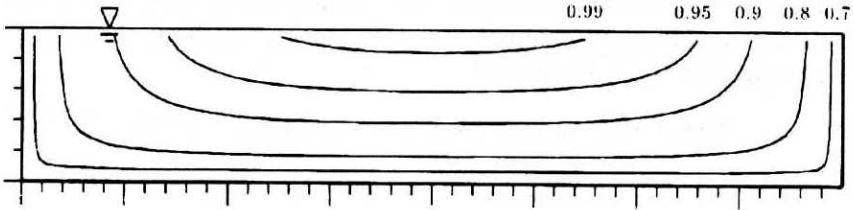
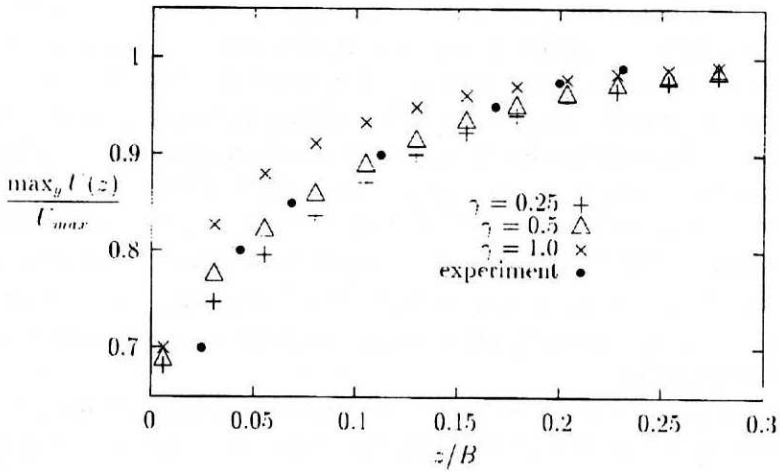**Fig. 5.** Contours plot for $U/U_{\max}(L_z/L_y = 1, \gamma - 0.5)$

Fig. 6. $\max_y U(z)/U_{\max}$ for $L_z/L_y = 1.0$

Vertical velocity profiles at the cross section axis of symmetry (in a zone of fully developed two-dimensional flow) are presented in Figure 7. It is seen that the computed velocity profile declines more from the log-law curve for $\gamma = 1$ than for smaller γ's. The choices $\gamma = 0.25$ and $\gamma = 0.5$ give very close results.
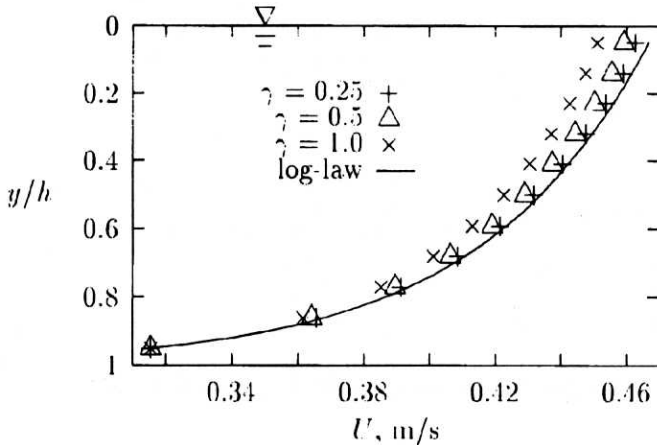

Fig. 7. $U(y)$ at $z = B/2$ for $L_z/L_y = 1.0$

Another point for discussion concerns dependence of the longitudinal pressure gradient $\bar{p}_x$ on parameter γ. For steady uniform flow in an open channel the pressure is hydrostatic and the average pressure gradient in a longitudinal direction should be zero. Calculations give $\bar{p}_x = -0.14$ for $\gamma = 0.5$ and $\bar{p}_x = 0.44$ for $\gamma = 0.5$. So they stand for the choice of γ of about 0.6.

Figure 8 shows vertical profiles of the eddy viscosity ν_{xy} at two distances from the sidewall for $\gamma = 0.5$. The solid line represents the theoretical parabolic curve for the eddy viscosity in a two-dimensional steady turbulent flow. It is in accordance with calculations at the centre of the channel but not near the side wall.

Figure 9 shows vertical distribution of the normalized Reynolds stress $\overline{u'v'}$. The solid line gives its two-dimensional theoretical linear distribution. At the channel centre ($z = B/2$) computed values for $\overline{u'v'}/u_*^2$ are seen to match the theoretical curve well, whereas near the wall ($z = B/10$) the profile is distorted due to the influence of the sidewall.

All the previous analysis leads to the conclusion that results for ($L_z/L_y = 1.0$, $\gamma = 0.5$ fit experimental data well. Very similar results are obtained for $L_z/L_y = 0.5$, $\gamma = 0.5$. They indicate that the model has low sensibility to L_z/L_y when it ranges from 0.5 to 1.0. Note in addition that the choice of $L_z/L_y = 1.0$
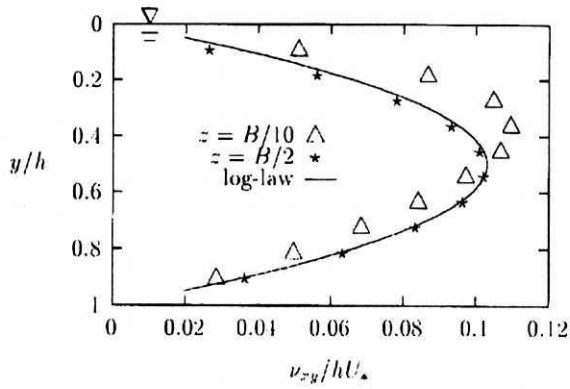
A. A. Rylov, W. Czernuszenko

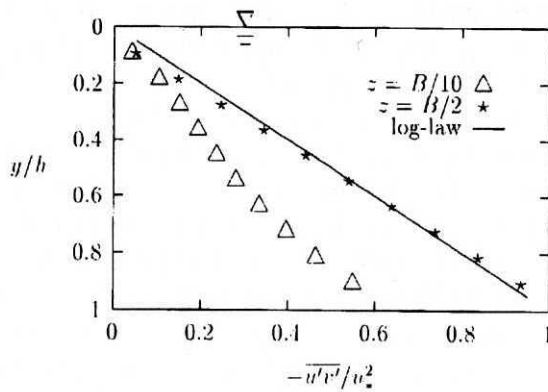**Fig. 8.** Eddy viscosity ν_{xy} for $L_z/L_y = 1.0, \gamma = 0.5$

Fig. 9. Shear stress $-\overline{u'v'}/u_*^2$ for $L_z/L_y = 1.0, \gamma = 0.5$

means that for this case turbulence is homogeneous since formulae (8)–(11), (14) give $l_x = l_y = l_z$.

5. Conclusions

1. The generalisation of Prandtl's mixing length model may be used to calculate velocity distribution in three-dimensional flows. The components of the mixing length tensor for open channel flows are specified based on the well-known formulae for mixing length in two-dimensional flows. Nikuradse's formula (13) is utilized to describe the lateral growth of the mixing length components in the edge zones and Eq. (12) deduced from the log-wake law – for their profiles in the vertical direction.

2. The Patankar & Spalding numerical procedure appeared to be quite adequate for the case in question. Due to its marching feature in a streamwise direction the procedure demands much less computational resources than solvers treating momentum equations as elliptical in the whole three-dimensional space domain, i.e. pertaining derivatives in a streamwise direction. Steadiness of turbulent flows under consideration permits the assumption of x-derivatives of stress tensor components to be negligible and to obtain parabolic approximation to the Reynolds equation.

3. The best agreement between measured and calculated velocity distributions for the steady turbulent flow in the rectangular channel is reached for homogeneous macroturbulence ($l_x = l_y = l_z$) when γ is close to 0.5.

4. The middle zone in the channel flow (eddy viscosity varies parabolically in the vertical direction and shear stress varies linearly against the distance from the bottom) stretches from the channel axis to the vertical profiles situated at a distance of 0.25 B from the side walls.

References

Czernuszenko W., Rylov A. A. (1997), A generalization of Prandtl's mixing length model for three-dimensional open channel flows, *Report IGF/G-28/5*, Inst. of Geophysics PAN, Warszawa.

Fletcher C. A. (1991), *Computational Techniques for Fluid Dynamics*, 2nd ed., Springer-Verlag.

Laudner B. E., Spalding D. B. (1974), The Numerical Computation of Turbulent Flow, *Comp. Meth. in Appl. Mech. and Eng.*, 3, 269–289.

Laudner B. E., Reece G. J., Rodi W. (1975), Progress in the development of a Reynolds stress turbulence closure, *J. Fluid Mech.*, 68, 537–566.

Leschziner M. A. (1980), Practical evaluation of three finite difference schemes for the computation of steady-state recirculating flows, *Comp. Meth. in Appl. Mech. Eng.*, 23, 293–312.

Naot D., Rodi W. (1982), Numerical simulations of secondary currents in channel flow, *J. Hydr. Div. ASCE*, 108, No. HY8, 948–968.

Nezu I., Nakagawa H. (1993), *Turbulence in Open-Channel Flows*, A. A. Balkema, Rotterdam.

Patankar S. V., Spalding D. B. (1972), A calculation procedure for heat, mass and momentum transfer in three-dimensional parabolic flows, *J. Heat Mass Transfer*, 15, 1787–1806.

Rastogi A. K., Rodi W. (1978), Prediction of Heat and Mass Transfer in Open Channel, *J. Hydr. Div. ASCE*, 104, No. HY3, 397–420.

Rodi W. (1980), *Turbulence Models and their application in hydraulics*, University of Karlsruhe.

Schlichting H. (1955), *Boundary Layer Theory*, McGraw Hill, London.

Tominaga A., Ezaki K., Nezu I., Nakagawa H. (1989), Three-dimensional turbulent structure in straight open channel flows, *J. Hydr. Res.*, 27, 149–173.

Yalin M. S. (1992), *River Mechanics*, Pergamon Press, Oxford.